Chapter 3
Investigation of Output Metrics for Dynamic Topology Optimization of PCB Reinforcement

Ryan Semler, John Bell, and Laura Redmond

Abstract Rigid-flex Printed Circuit Board (PCB) robotics have been considered as a future architecture for the exploration of high-risk extraterrestrial environments such as the moon. One major challenge with this architecture is the lack of modeling methodologies and design strategies for the use of PCB as the primary structure of the system. Previous research has established the need for external reinforcement on PCB panels to survive the expected dynamic loading for an extraterrestrial mission. Because the primary advantages of the system are low mass and cost-effectiveness, topology optimization is a prime candidate for the design of lightweight exoskeletons to reinforce the PCB structure. This paper begins to formulate a code to interact with the commercial software Abaqus to formulate custom Equivalent Static Loads (ESLs) and output metrics that control the optimization of a reinforcing exoskeleton for a PCB panel subjected to dynamic loads. First, the paper outlines several methods for selection of ESLs in the literature. Second, common failure mechanisms of PCB are presented to inform the parameters that are investigated in the study. Third, the algorithm for generating the ESL and to pass customized parameters to the Abaqus TOSCA solver is presented. Fourth, preliminary results are presented to demonstrate the optimization routine when optimizing for the output metric of strain energy. The paper concludes with future various output metrics to be used to inform the optimization, and the presentation will include recommendations for the dynamic topology optimization of PCB structures based on the findings in this case study.

Keywords topology optimization · dynamic analysis · PCB

Introduction

NASA JPL's rigid-flex PCB Pop-Up Folding-Flat Explorer Robot (PUFFER) was originally designed to be a lightweight, cost-efficient explorer robot for Mars, which included Nomex fabric joints to improve the fatigue resistance of the rover [1]. Clemson University has collaborated with NASA JPL to develop modeling methodologies for rigid-flex PCB robotics validated with dynamic testing to be used for investigations of potential loading scenarios to PUFFER if it were used for a Lunar scouting mission. This research determined that the current PUFFER structure is inadequate for an 80-meter drop into a lunar pit [2–5] and that external reinforcing would be needed to preserve large panel sizes. Research has also been conducted to optimize a reinforcing skeleton on a single-degree of freedom (SDOF) model of a PCB panel with a frequency-based approach [6]. The frequency-based optimization prioritized minimizing displacement while constraining the mass to be less than or equal to 100% and utilized a looping process to conduct the optimization multiple times as the system's natural frequency shifted during optimization.

This work furthers the research on the structural reinforcement by leveraging commercial software to conduct the opti-

Ryan Semler
School of Civil, Environmental Engineering and Earth Sciences, Clemson University, Clemson, SC 29631
e-mail: rsemler@clemson.edu

John Bell, Ph.D.
NASA Langley, Hampton, VA 23666
e-mail: john.bell@nasa.gov

Laura Redmond, Ph.D., Associate Professor
School of Civil, Environmental Engineering, and Earth Sciences, School of Mechanical and Automotive Engineering, Clemson University, Clemson SC 29631
e-mail: lmredmo@clemson.edu

Chad Walber et al. (eds.), *Sensors & Instrumentation and Aircraft/Aerospace Testing Techniques, Vol. 8*, Conference Proceedings of the Society for Experimental Mechanics Series, https://doi.org/10.13052/97887-438-0153-5_3

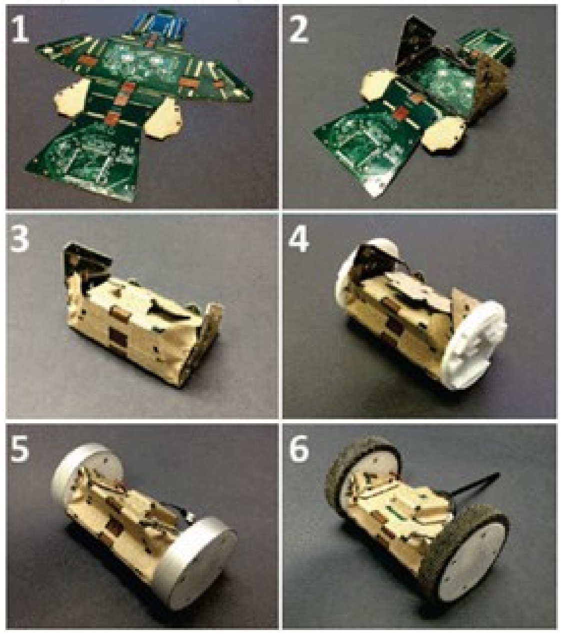

Fig. 1 Rigid-flex NASA JPL rover, PUFFER [1]

mization process with various output metrics on a multi-degree of freedom (MDOF) system utilizing the Equivalent Static Load (ESL) approach to determine loads at each iteration of the optimization. This preliminary case study presents the first step in this investigation with a baseline sizing optimization of the reinforcement after applying a random base excitation to the system. The overall goals of this paper are to 1) present the ESL method and integration with Abaqus TOSCA to conduct the optimization process, 2) present the various parameters to be considered for the objective function in PCB exoskeleton design and possible formulations of the ESL, and 3) show preliminary results of the optimization routine for a baseline set of optimization parameters.

ESL Generation in Literature

There exist several methods of creating static-equivalent loads (ESLs) from dynamic loading. The most common method is a time-domain approach in which the static-equivalent loads are calculated using the stiffness matrix and dynamic displacements at a specific time point. Choi & Park examine an analytical method that utilizes this approach with a transient analysis for displacements and generates ESLs at all locations within a model [7]. Park then applies this approach to a structural optimization problem by generating ESLs from a displacement field at each time step of the dynamic analysis [8]. In later years, Jang et al. have used this approach for dynamic response topology optimization in the time domain [9, 10].

Preliminary research shows that a frequency-based approach can be utilized with commercial software to derive approximate static-equivalent loads for dynamic topology optimization of a single-degree of freedom system subjected to sinusoidal loads [6]. The approach generates static-equivalent loads as a load which generates mode 1 deformations modified by a dynamic response amplification factor, R_d. This factor is calculated from the applied excitation frequency and the natural frequency of the system. The approach was verified at each intermediate step of the optimization by comparing the results from the ESL(s) to the maximum steady-state response of the model run in time domain with the sinusoidal base excitation. For the single degree-of-freedom system approach, a mode participation of 80-90% is sufficient for determining the dynamic response of the structure [11]. However, this approach is limited to sinusoidal loading.

Static-equivalent loads are typically approximated for optimization problems with displacement or stress. Displacement-based approximations use inequalities to calculate ESLs that are then optimized to find the smallest load at a critical time [7]. Stress-based approximations utilize stress as a constraint condition when calculating ESLs. This is because displacement and stress are not proportional when a rigid body is dominant in the displacement component due to the internal strains of the body being negligibly small [7].

A time step for equivalent static loads is selected based on the type and objective of the analysis or optimization problem. For a minimization problem, the time step is usually chosen at the point at which the objective function, usually displacement or stress, is at its maximum. ESLs are calculated from the dynamic displacement field at this specific time step [7]. This method of time step selection prioritizes a single time point for a single area of a model. In this work, the analytical method for obtaining the ESL will be utilized, and we will later investigate whether selecting the time point based on localized maxima around critical mounted components or selecting it based on global maxima results in a more robust design for the PCB exoskeleton.

PCB Failure Mechanisms

A plethora of research studies have been conducted to identify, investigate, and mitigate several failure mechanisms present in PCB panels. Such failure mechanisms include Conductive Anodic Filament (CAF), cracking, and solder joint failure. CAF is an iterative failure induced by PCB depenalization, primarily due to moisture exposure caused by small cracks and the formation of dendrite, which leads to burn-out of the panel [12]. Cracking is a corrosion-induced failure due to the presence of dendrite growth [13]. Dendritic growth is an electrochemical phenomenon resulting in conductive metal filaments forming along the PCB panel; it is most notably caused by high relative humidity and contamination [14]. In a dynamic environment, PCB panels can fail when the yield stress of a ply is exceeded from board deformation. These deformations can be caused by shock waves or stress distributions generated from impact, vibration, or panel bending. Differential flexing and elongation of the board may damage sensitive interconnections [15–17].

Solder joint failure itself has several potential causes. They are critical components of PCB panels as they anchor physical components to the panel and can provide essential electrical connection to the PCB itself. Manufacturing errors and unsatisfactory environmental conditions can result in failure. However, the most prominent cause of solder joint failure is cracking due to dynamic flexing as the stress in the solder joint exceeds the joint strength. Drop impacts, for example, may produce panel differential bending and/or large inertial forces from the heavier mounted components that induce severe stresses in the solder joints [18]. As such, the use of stress and curvature as objective functions within the optimization routine will be examined.

Summary of Optimization Parameters to be Investigated

The optimization parameters investigated are outlined in Table 1. ESL time point selections for global (full model) and local (partial model) areas will be examined for maximum principal stress (abs.), maximum curvature, and both stress and curvature simultaneously. The preliminary case study examines a global determination of the ESL time point for maximum strain energy as a whole model quantity for the initial baseline analysis to demonstrate the optimization routine.

Table 1 Matrix of output metrics

	ESL time point selection method	
	Single time point, single area	Multiple time points and areas
Output metric measured	Whole model strain energy(abs.)	
	Maximum element strain energy over whole model	Maximum element strain energy near each component
	Maximum curvature	Maximum curvature
	Max. principal stress (abs.)	Max. principal stress (abs.) near each component

**Blue represents the subset shown in this abstract, green is the additional data that will be presented at IMAC, and grey are suggested metrics for future investigations*

Table 2 System Material Properties

	Density [tonne/mm^3]	Young's modulus [MPa]	Poisson's ratio [-]
FR4 [19]	1.85E-09	18,500	0.136
Stainless Steel 316L	8.00E-09 [20]	193,000 [20]	0.28 [21]
Electronic Component^a	1.97E-07	N/A	N/A

^{a}Density is a reasonable approximation for instrumentation on a planetary robot. Stiffness is unaccounted for

Model Setup

A finite element model (FEM) was created based on an instrumented PCB panel for modal testing and model correlation shown in Figure 2 [19]. The model was modified to add three representative electronic components by increasing the density of certain areas of the panel where they could be located. A system can be idealized as an SDOF system if the natural mode has a modal participation of at least 80%, meaning it captures the majority of the system's dynamic response with one mode. The components are arranged in such a way that the system is a multiple degree-of-freedom (MDOF) system that cannot be idealized as an SDOF system due to the necessity of multiple modes to increase the modal participation.

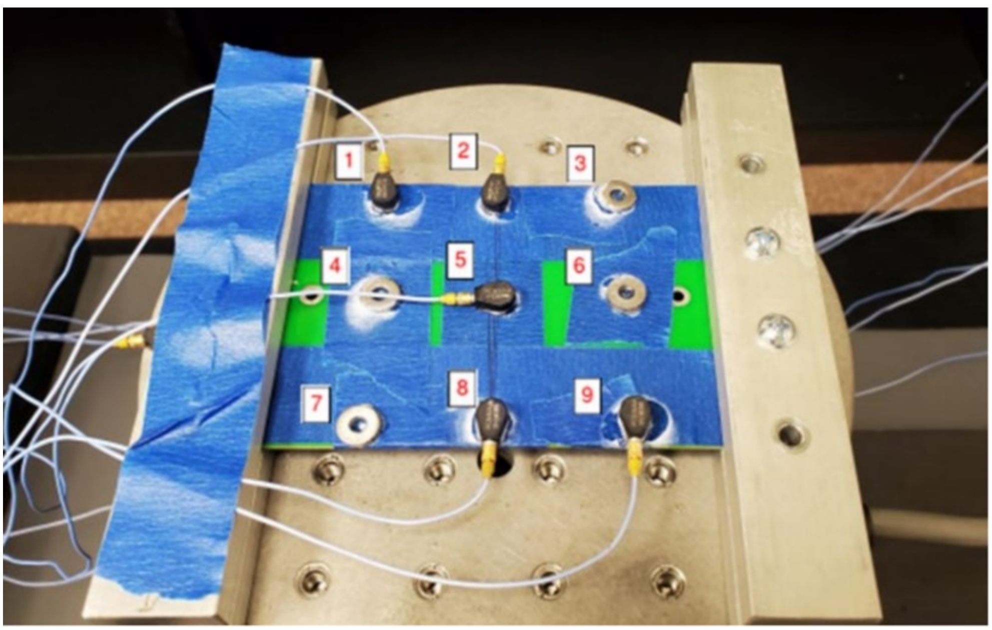

Fig. 2 Instrumented PCB panel for fixed—fixed frequency test [18]

Figure 3 shows the layout of the 150 mm x 75 mm PCB panel. The PCB panel has a thickness of 1.5 mm, and the reinforcement (not shown) of the same area has a thickness of 6.35 mm. The portion of the PCB & reinforcement shown in orange is clamped to account for physical testing situations. Tie constraints between the PCB panel and reinforcement are shown in dark blue. The area of the representative electronic components, shown in maroon, is varied to induce an MDOF system and to emulate the varying size of physical instrumentation. A reinforcement layer consisting of an isotropic, printable material (Stainless Steel 316L) was added and constrained to the PCB panel with several ties representing physical fasteners. The shape of this reinforcing layer will be optimized to minimize the objective function in each scenario. The reinforcement is shown on the PCB in Figure 4. The material properties of the model are denoted in Table 2.

Time History Excitation

A random base motion excitation is applied to the clamped regions of the system through an acceleration time history generated from a power spectral density curve. Table 3 provides the input power spectral density, which uses values converted into the model units from the General Environmental Verification Standard (GEVS) for GSFC Flight Programs and Projects [22].

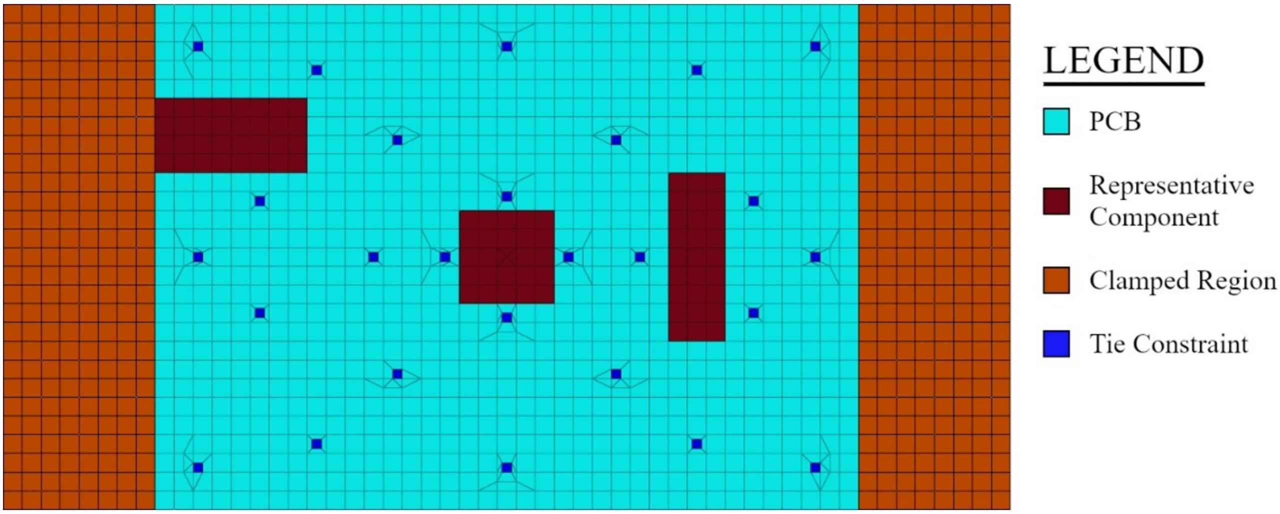

Fig. 3 PCB panel layout

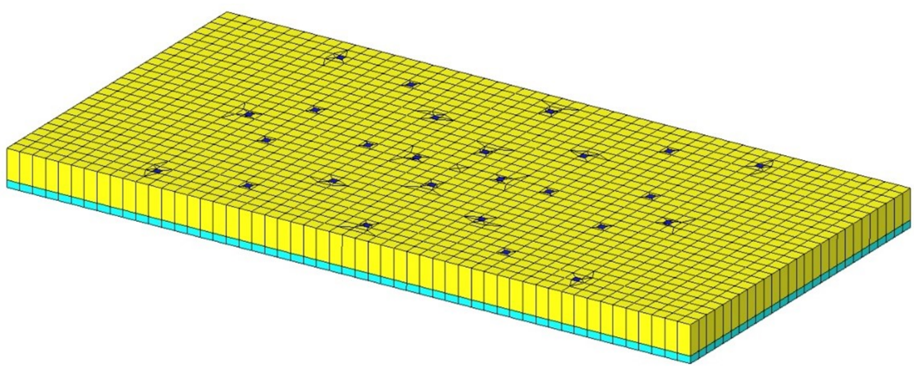

Fig. 4 PCB model with reinforcement (yellow)

Table 3 Power spectral density inputs

Frequency (Hz)	Amplitude (mm^2/s^3)
20	2500430.0
50	15387261.5
800	15387261.5
2000	2500430.0

The PSD was used to generate a time history for the optimization process such that a time step in the simulation could be selected for the calculation of static-equivalent loads. The time history was synthesized as a series of sinusoids resembling a random signal and satisfying the specified PSD [23]. A custom MATLAB script was created to calculate the amplitudes of the specified PSD and sum the spectral components at each time point. The time history was verified to fit the PSD visually in Figure 5 using Welch's method in MATLAB with a window division length of 6 as well as 15 samples of overlap between segments. The GRMS values between the time history and input power spectral density were found to be 14.163 g's and 14.136 g's, respectively, with a reasonably small difference of 0.19%. Then, a normalized PDF, shown in Figure 6, was plotted to verify the generated time history followed a Gaussian distribution. The bin width for the histogram was 0.038. The kurtosis was found to be 2.9932; since this is very close to 3, it can be said that the generated time history follows a normal or Gaussian distribution similarly to the power spectral density input.

The modal damping ratio was approximated based testing conducted on solid PCBs by Bell et. al [4] and were calculated using the half power bandwidth method [24]. The estimated damping ratio from these experiments ranged from 1.26% to 1.82% for the first three modes in a clamped condition. Thus, for the first 50 modes of our model, a damping ratio of 1.5%

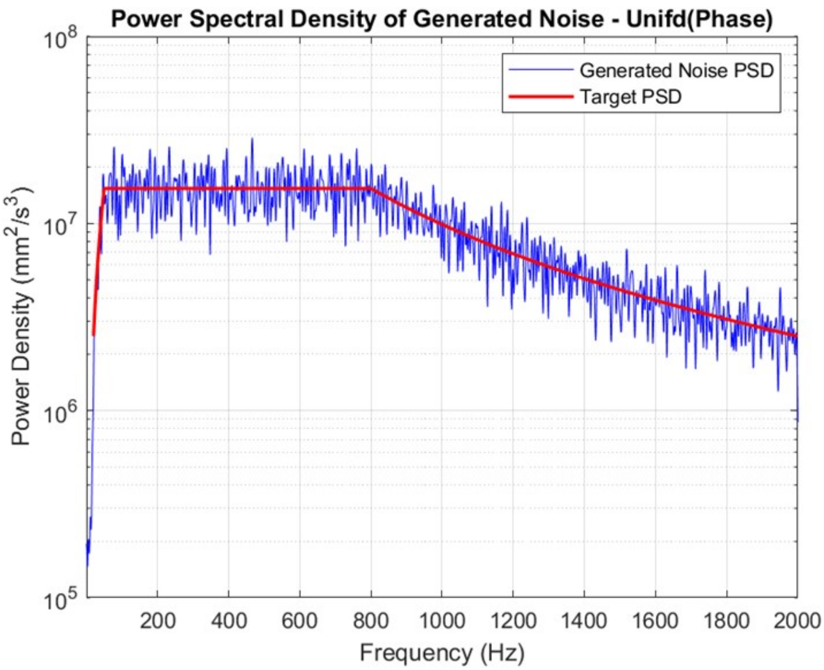

Fig. 5 Input power spectral density (red) vs time history (blue)

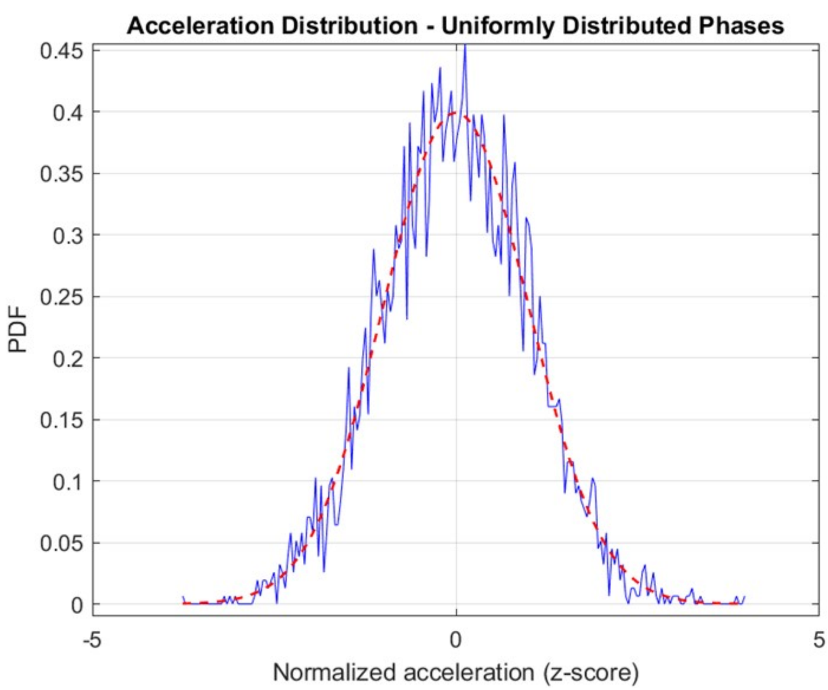

Fig. 6 True Gaussian distribution (red) vs normalized Gaussian PDF of time history (blue)

was applied for each mode as a reasonable estimate of damping. For reference, the fundamental frequency of the baseline model with uniform reinforcement thickness was 1193.1 Hz.

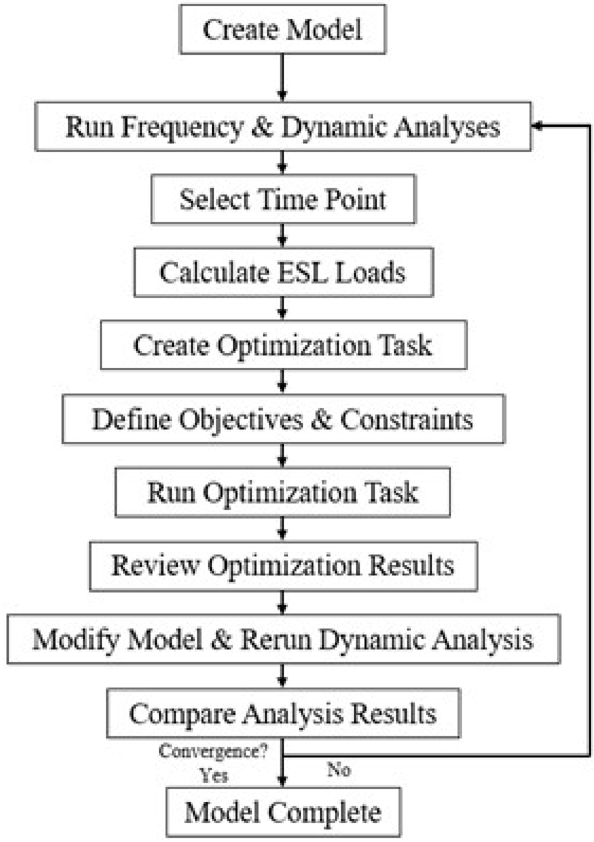

Fig. 7 Optimization procedure

Optimization Routine and Code

The optimization method followed is an iterative process in which the reinforcement panel is repeatedly optimized until the results are satisfactory. The full optimization process is outlined in the following flow chart.

Several scripts were written and utilized throughout the process. Most prominently, a script was written to extract the displacement history data from the dynamic analyses results for use in calculating the static-equivalent loads for the system at the specified time step. The calculation of the equivalent-static loads itself was carried out with a separate MATLAB script. The optimization task was a general (sensitivity-based) optimization of the reinforcement exoskeleton with default settings modified to freeze the boundary regions, unfreeze the load regions, and allow for 0.5 (50%) maximum change per cycle. Sizing optimization was used in lieu of topology optimization for the preliminary case study to ensure applied ESLs were unaffected by the deletion of elements throughout the process. For the sizing optimization, a thickness control was defined for the reinforcement to allow the thickness of its elements to change from 0.635 mm (10% thickness) to 12.7 mm (200% thickness). The objective function is defined as the selected output metric to be measured, and the constraint limits the mass to less than or equal to 100% of its initial mass. For consistency within the optimization loop, the mass was kept consistent between iterations by increasing the thickness of the remaining reinforcement after remodeling. The proposed optimization process output metric comparison matrix was outlined in Table 1. The preliminary case study presents the results of the first round of optimization with whole element strain energy as the output metric and a single time point, single area ESL generation method. The time point chosen was the time at which strain energy in the model was maximum.

Sample Results

In this preliminary case study, the optimization task was used to optimize the reinforcement exoskeleton to minimize the strain energy globally. The mass of the system remained unchanged throughout the process for consistency when comparing

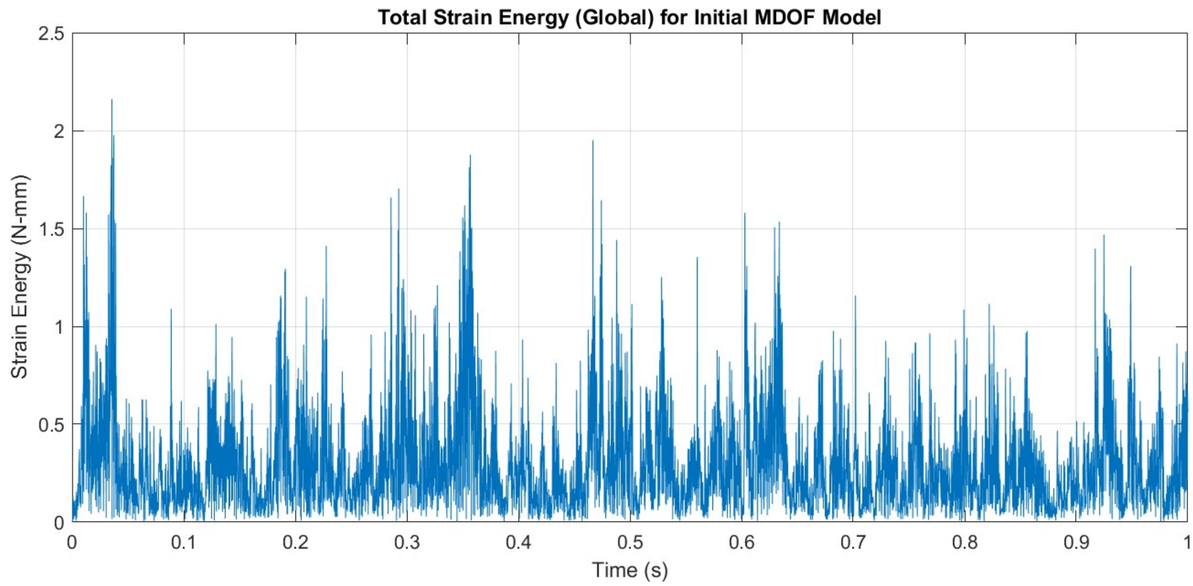

Fig. 8 Total strain energy over time (global) for initial MDOF model

results. Equivalent-static loads used for the optimization were calculated from the stiffness and displacements due to the time history random base excitation at the critical time point which strain energy was maximum. These loads were applied to the model at every node. Figure 8 shows the strain energy in the baseline model (uniform reinforcement) at all time points due to the random base excitation. The critical time point was found to be 0.0356 s with a strain energy of 2.161 N-mm.

The result of the first round of optimization is shown in Figure 9. Clamped reinforcement is hidden for clarity. As anticipated, reinforcement was removed at areas where overall density was lower. The reinforcement primarily remained where strain energy was higher in the model, which is where density was higher in the PCB panel due to the components. Note that even though mass was permitted to decrease during the optimization routine in TOSCA, the optimization preserved about 99% of the original system mass. This optimization result was remodeled to adjust the thickness of the indicated reinforcement elements, which were modified rather than deleted for consistency between runs and to allow for the strain energy of the remade model to be compared to the previous model with the same ESLs.

The remade model, shown in Figure 10, was found to have a reduced strain energy of 2.126 N-mm for the ESL generated with the baseline model. In the model, the red region has a thickness of 12.7 mm, the blue region has a thickness of 0.635 mm, and the orange region to be optimized has a thickness of 5.816 mm. The thickness of the orange region to be optimized was adjusted so the total mass of the system remained unchanged. The yellow region represents the reinforcement that is clamped and unoptimized. The same random base excitation was applied to the first-round optimized model to determine the critical time point and maximum strain energy for the next step in the optimization procedure. Figure 11 shows the maximum strain energy in the model at all time points of the analysis. The critical time point was found to be 0.0356 s with a maximum strain energy of 2.262 N-mm. Note the total strain energy slightly increased from the initial model as dynamic properties of the system have shifted.

The result of the second round of optimization is shown in Figure 12. Clamped reinforcement is hidden for clarity. Like the first optimization run, the thickness of reinforcement within the region to be optimized was increased in areas where the overall density was higher and decreased where it was lower. This optimization result was remodeled in a manner similar to that of the remodel of the previous optimization result, though the regions of maximum thickness at isolated regions from the previous result were modified to reflect the thickness of nearby regions instead due to the second optimization result representing a final run.

The model remade from the second and final round of optimization is shown in Figure 13. Unlike the previous model, the orange region now has a reduced thickness of 5.320 mm. This model was found to have a reduced strain energy of 2.236 N-mm when analyzing it with the ESLs generated from the previous model run. The model was also found to have the same strain energy as the previous model of 2.383 N-mm when analyzing it dynamically. Thus, overall, the whole model strain energy was relatively flat throughout the optimization process and slightly increasing as the dynamics of the system changed. It is likely not an ideal optimization parameter. A summary of the progression of the whole model strain energy values throughout the optimization process is shown in Table 4.

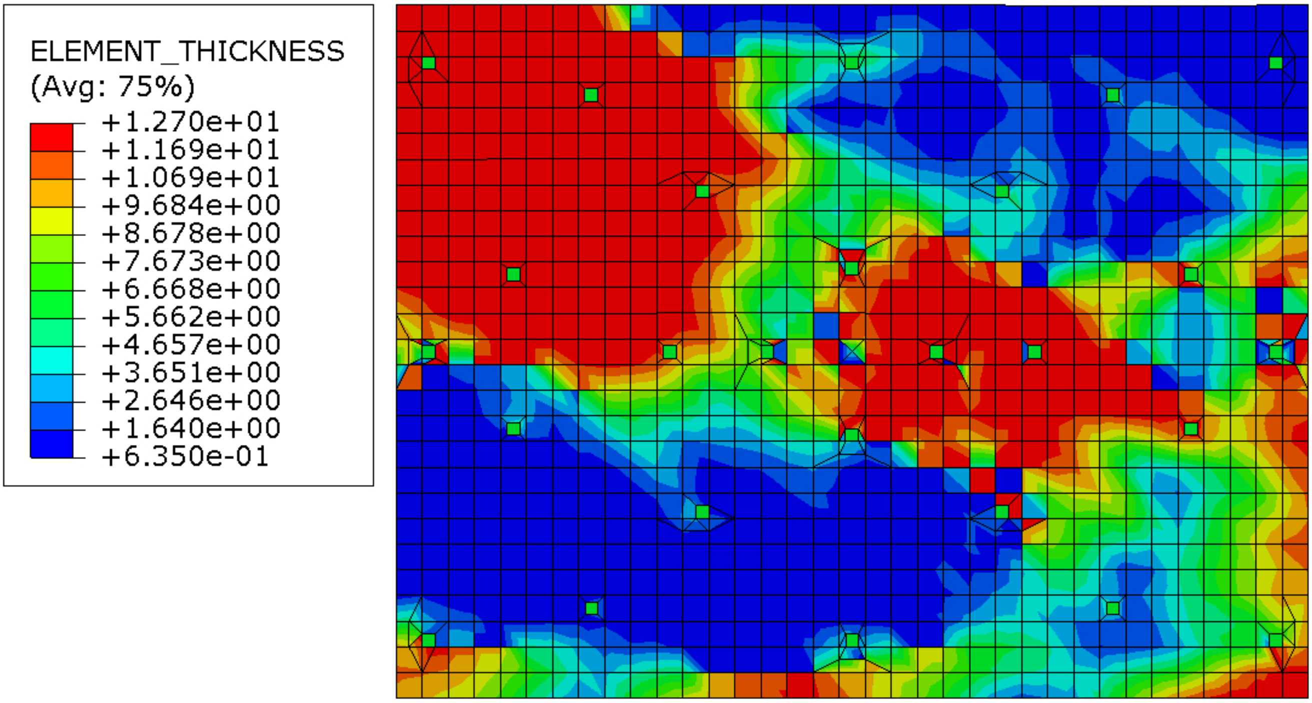

Fig. 9 First-round optimization result (element thickness of the reinforcement layer)

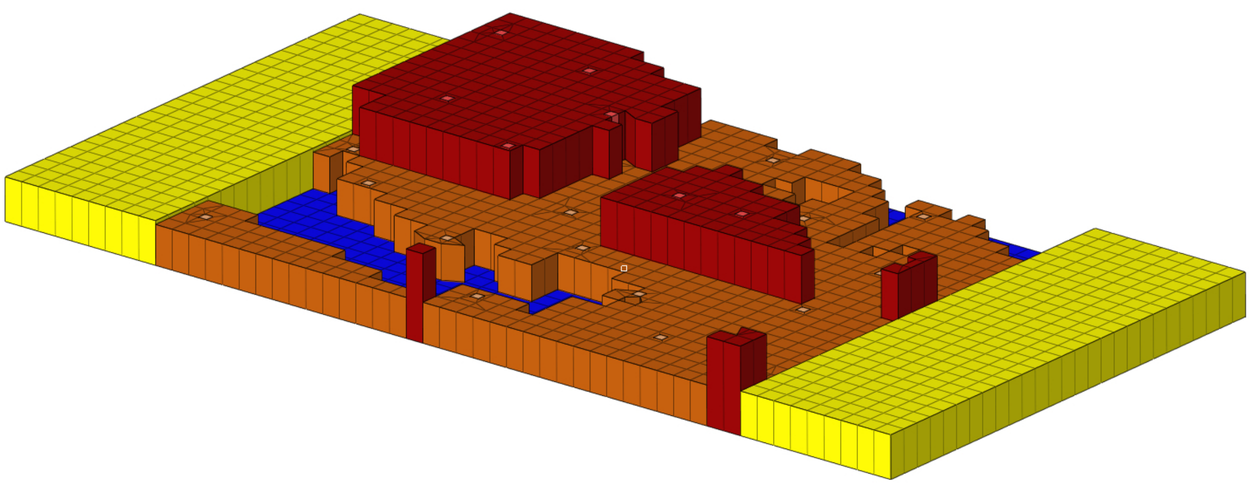

Fig. 10 Remodel of first-round optimization result (reinforcement only)

A final comparison was made between the strain energy in the PCB without reinforcement and the second-round optimization result to verify that reinforcement was at least beneficial in reducing the whole model strain energy. Without reinforcement, the maximum strain energy in the PCB alone is 106.421 N-mm when analyzing it with the same time history random base excitation, which is monumentally higher than that of the reinforced PCB. The strain energy over time for the unreinforced PCB is shown in Figure 15.

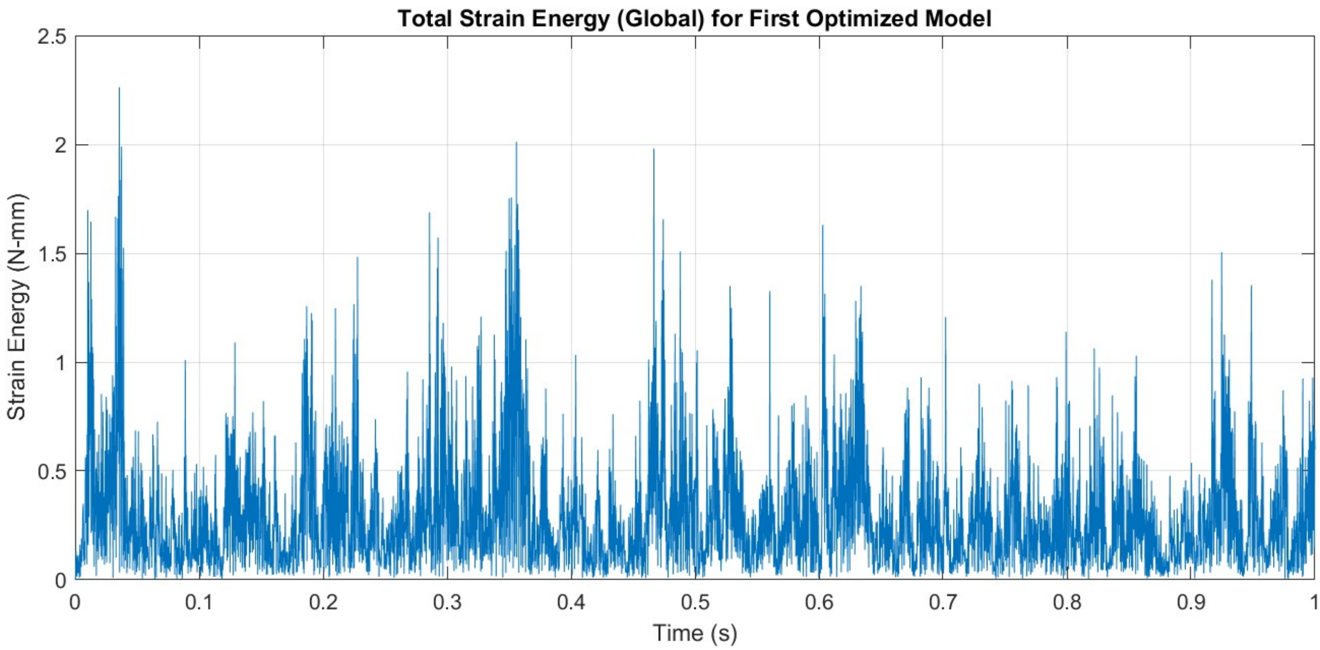

Fig. 11 Total strain energy over time (global) for first optimized model

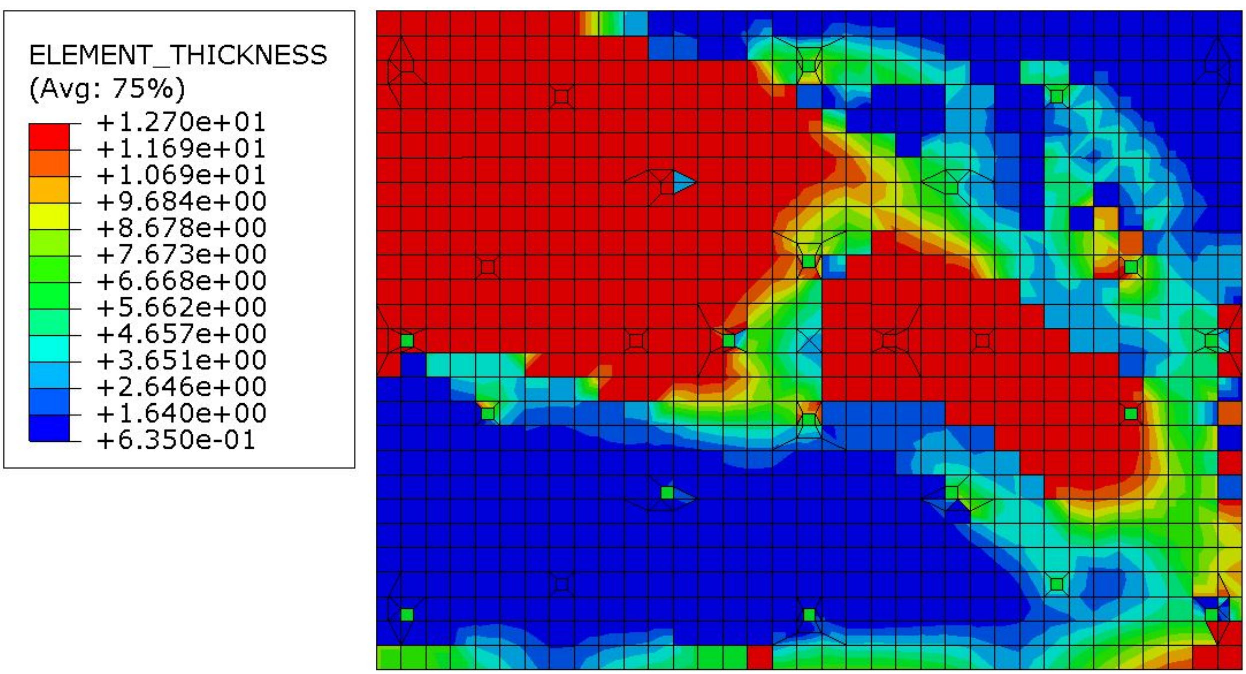

Fig. 12 Second-round optimization result: reinforcement (green) and component locations (red)

Conclusions and Future Work

The preliminary case study work has shown that the dynamic topology optimization process presented results in a non-uniform optimized structural reinforcement with a significant reduction in the objective function. The conference presentation will include and compare results for the outputs that can be included by default in the TOSCA solver and compare the use of global vs. localized regions for identifying the critical time point(s) for ESL(s). The presentation will additionally introduce a method of extracting custom output metrics from Abaqus. Future work will include utilizing custom optimization

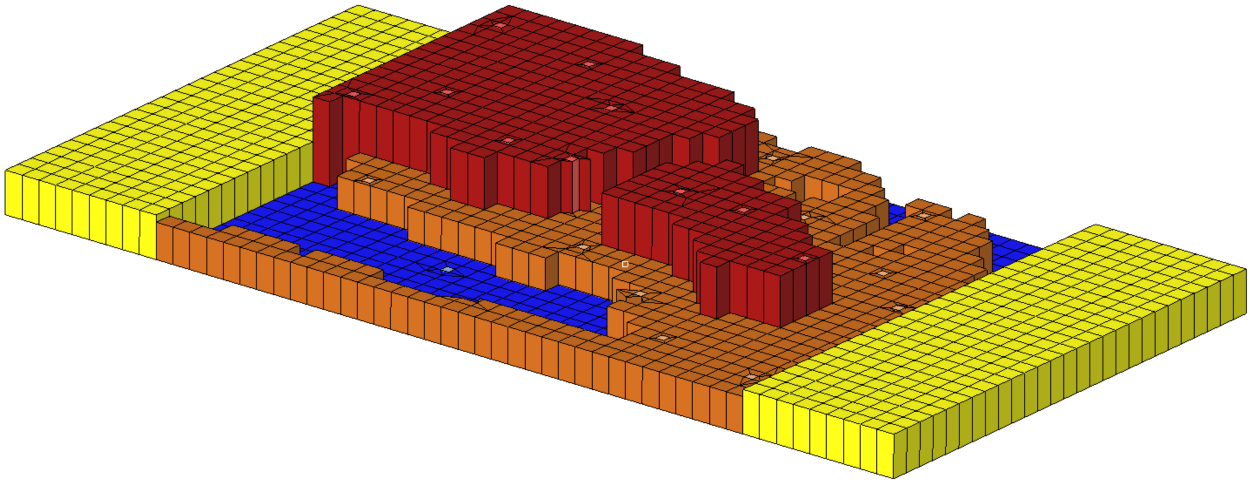

Fig. 13 Remodel of second-round optimization result (reinforcement only)

routines to leverage the custom output metrics as objective functions and experimental testing to validate that the optimized reinforcement performs as expected.

Acknowledgments This work performed as part of a NASA South Carolina Space Grant Consortium Graduate Research Assistantship, Award # 80NSSC20M0054, Subaward # 20-013-GRF-CU-017.

References

1. Karras, J.T., Fuller, C.L., Carpenter, K.C., Buscicchio, A., McKeeby, D., Norman, C.J., Parcheta, C.E., Davy-dychev, I., Fearing, R.S.: Pop-up Mars rover with textile-enhanced rigid-flex PCB body. In: 2017 IEEE International Conference on Robotics and Automation (ICRA) (2017). https://doi.org/10.1109/icra.2017.7989642
2. Bell, J., Redmond, L., Carpenter, K., and de la Croix, J.P., "Finite Element Modeling of Rigid-Flex Printed-Circuit-Board Origami Robotics Subjected to Large-Scale Deformations," AIAA Journal, 62(4), 2024. https://doi.org/10.2514/1.J062738
3. Bell, J., Redmond, L., Carpenter, K., de la Croix, J.P.: Experimental dynamic characterization of rigid-flex PCB systems. Exp. Tech. (2022). https://doi.org/10.1007/s40799-022-00559-4
4. Bell, J., Redmond, L., Carpenter, K., de la Croix, J.P.: Finite element modeling of rigid-flex PCB robotic structures for dynamic environments. J. Microelectron. Electron. Packag. **19**(1) (2022)
5. Bell, J., Redmond, L., Carpenter, K., de la Croix, J.P.: Design of rigid-flex PCB robotics leveraging validated finite element simulations. In: IEEE Aerospace, Big Sky, MT, 5–12 Mar 2022
6. Semler, R., Carlson, D., Crowder, J., & Redmond, L., "Dynamic Topology Optimization of Rigid-Flex PCB Robotic Systems," *IMAC XLII*, Orlando, FL, January 29-Febuary 1, 2024.
7. Choi, W.-S., Park, K. B., & Park, G. J. (2005). Calculation of equivalent static loads and its application. *Nuclear Engineering and Design*, *235*(22), 2337–2348. https://doi.org/10.1016/j.nucengdes.2005.05.030
8. Park, G.-J. (2005). *Structural Optimization Using the Equivalent Static Load Concept*. https://doi.org/10.21236/ada451871
9. Jang, H. H., Lee, H. A., and Park, G. J., "Dynamic Response Topology Optimization Using Equivalent Static Loads," 8th World Congress on Structural and Multidisciplinary Optimization, Lisbon, Portugal, June 1–5 2009.
10. Jang, H. H., Lee, H. A., Lee, J. Y., & Park, G. J. (2012). Dynamic Response Topology Optimization in the Time Domain Using Equivalent Static Loads. *AIAA Journal*, *50*1, 226–234. https://doi.org/10.2514/1.j051256
11. Priestley, M. J. N., Seible, F., & Calvi, G. M. (1996). *Seismic Design and Retrofit of Bridges*. John Wiley & Sons, Inc., p. 242.
12. Tan, C.-M., Chen, H.-H., Wu, J.-P., Sangwan, V., Tsai, K.-Y., & Huang, W.-C. (2022). Root Cause Analysis of a Printed Circuit Board (PCB) Failure in a Public Transport Communication System. *Applied Sciences, 12*(2), 640. https://doi.org/10.3390/app12020640
13. Lu, L. N., Huang, H. Z., Su, X. X., Wu, B. Y., & Cai, M. (2009). Investigation on PCB related failures in high-density electronic assemblies. *2009 International Conference on Electronic Packaging Technology & High Density Packaging*, 128–132. https://doi.org/10.1109/icept.2009.5270780
14. Singh, P., Sunder, M., Campbell, E., & Palmer, L. (2020). A Case Study of Nickel Dendritic Growth on Printed-Circuit Boards. *2020 Pan Pacific Microelectronics Symposium (Pan Pacific)*, 1–8. https://doi.org/10.23919/panpacific48324.2020.9059398
15. Chong, D. Y. R., Che, F. X., Pang, J. H. L., Xu, L., Xiong, B. S., Toh, H. J., & Lim, B. K. (2008). Evaluation on influencing factors of Board-Level drop reliability for chip scale packages (Fine-Pitch Ball Grid array). *IEEE Transactions on Advanced Packaging, 31*(1), 66–75. https://doi.org/10.1109/tadvp.2007.908024
16. E. H. Wong, K. M. Lim, N. Lee, S. Seah, C. Hoe and J. Wang, "Drop impact test - mechanics & physics of failure," 4th Electronics Packaging Technology Conference, 2002., Singapore, 2002, pp. 327-333, doi: 10.1109/EPTC.2002.1185692.

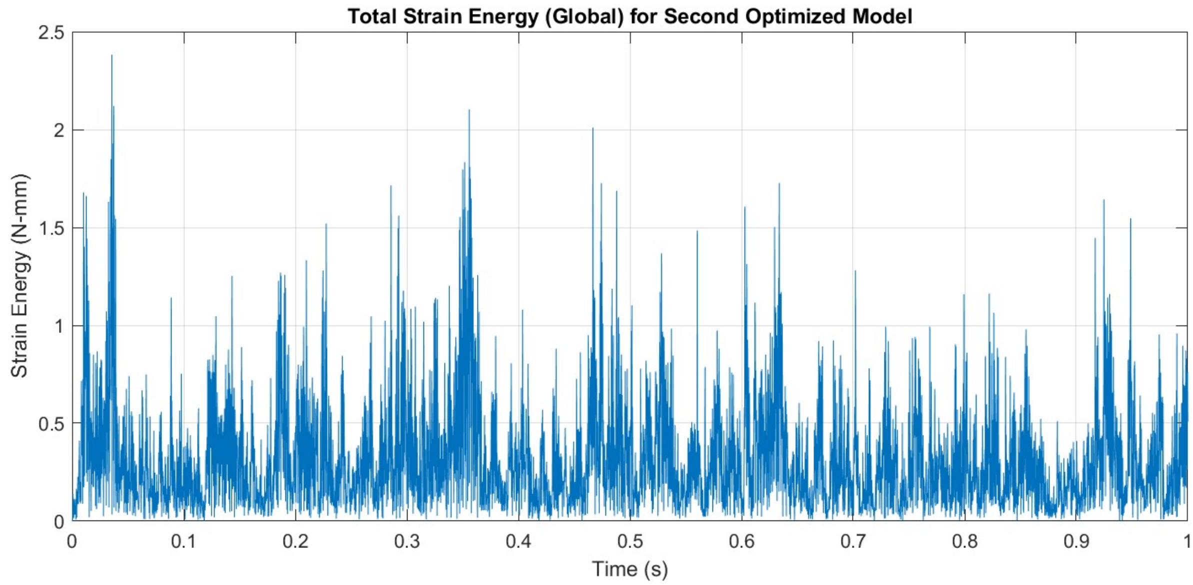

Fig. 14 Total strain energy over time (global) for second optimized model

Table 4 Summary of whole model strain energy progression throughout optimization process

Model iteration	Load description	Maximum whole model strain energy (N-mm)
Baseline model (solid uniform reinforcement)	ESL 1 (from initial time history analysis with Baseline Model)	2.161
First-round optimization model	ESL 1	2.126
First-round optimization model	ESL 2 (from time history analysis with first-round optimization model)	2.262
Second-round optimization model	ESL 2	2.236
Second-round optimization model	ESL 3 (from time history analysis with second-round optimization model)	2.383

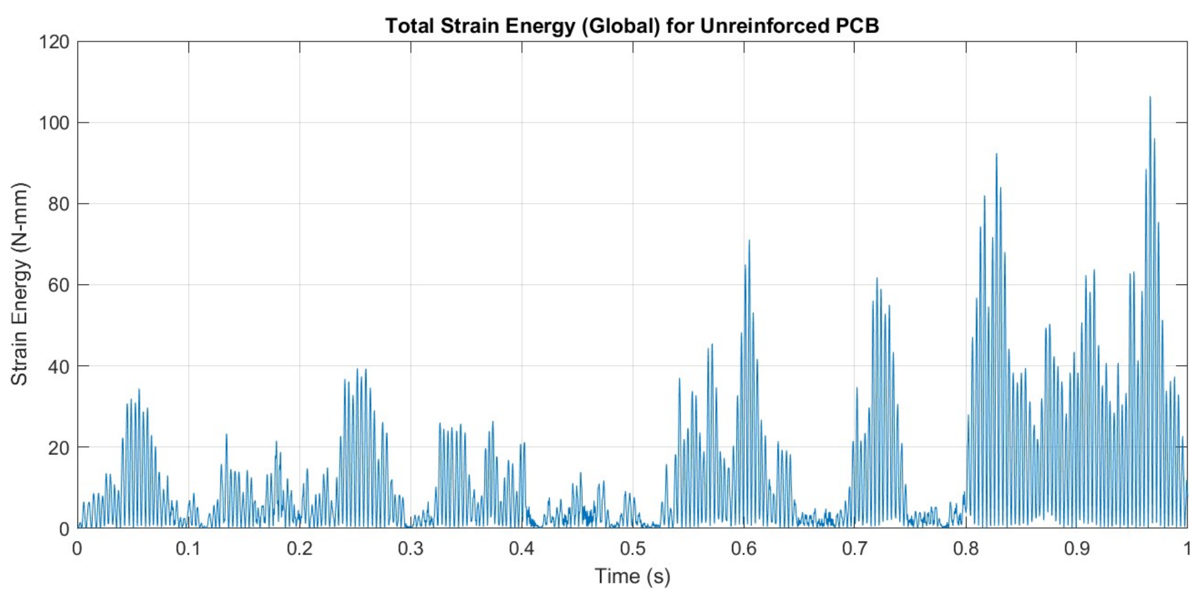

Fig. 15 Total strain energy over time (global) for initial MDOF model without reinforcement

17. Yang, Ping & Li, Wei. (2009). Numerical analysis on thermal characteristics for chip scale package by integrating 2D/3D models. International Journal of Numerical Modelling: Electronic Networks, Devices and Fields. 22. 43 - 55. 10.1002/jnm.694.
18. Gu Jie, Lim, C. T., & Tay, A. A. O. (2004). Modeling of solder joint failure due to PCB bending during drop impact. *Proceedings of 6th Electronics Packaging Technology Conference (EPTC 2004) (IEEE Cat. No.04EX971)*, 678–683. https://doi.org/10.1109/eptc.2004.1396694
19. Crowder, J.: Vibration fatigue of leaded solder joint interconnections for PCB electronics. M.S. thesis. Clemson University (2023)
20. AISI Type 316L Stainless Steel, annealed bar. ASM Material Data Sheet. (2022, March 22). https://asm.matweb.com/search/SpecificMaterial.asp?bassnum=MQ316Q
21. Tümer, D., Güngörürler, M., Havıtçıoğlu, H., & Arman, Y. (2020). Investigation of effective coating of the Ti–6Al–4V alloy and 316L stainless steel with graphene or carbon nanotubes with finite element methods. *Journal of Materials Research and Technology, 9*(6), 15880–15893. https://doi.org/10.1016/j.jmrt.2020.11.052
22. NASA, G. S. F. C., "General Environmental Verification Standard (GEVS) STD 7000B," Tech. rep., NASA GSFC-STD-7000B, 28 April, 2021.
23. Irvine, T. (2001). *Unit12* [PDF]. Vibrationdata. https://www.vibrationdata.com/Course_Units/UNIT12.pdf
24. Irvine, T. (2005). *THE HALF POWER BANDWIDTH METHOD FOR DAMPING CALCULATION* [PDF]. Vibrationdata. https://www.vibrationdata.com/tutorials2/half_power_bandwidth.pdf